Development of FAMD Code to Calculate the Fluid Added Mass and Damping of Arbitrary Structures Submerged in Confined Viscous Fluid

Gyeong-Hoi Koo*, Jae-Han Lee
Korea Atomic Energy Research Institute, P.O. Box 105, Yusong, Taejon 305-600, Korea

In this paper, the numerical finite element formulations were derived for the linearized Navier-Stokes' equations with assumptions of two-dimensional incompressible, homogeneous viscous fluid field, and small oscillation and the FAMD (Fluid Added Mass and Damping) code was developed for practical applications calculating the fluid added mass and damping. In formulations, a fluid domain is discretized with C^0-type quadratic quadrilateral elements containing eight nodes using a mixed interpolation method, i.e., the interpolation function for the velocity variable is approximated by a quadratic function based on all eight nodal points and the interpolation function for the pressure variable is approximated by a linear function based on the four nodal points at vertices. Using the developed code, the various characteristics of the fluid added mass and damping are investigated for the concentric cylindrical shell and the actual hexagon arrays of the liquid metal reactor cores.

Key Words: Fluid Added Mass, Fluid Damping, Finite Element Method, Viscous Fluid, Navier Stokes' Equation, Liquid Metal Reactor, Core Seismic Analysis

1. Introduction

A liquid metal fast breeder reactor (LMFBR) core is composed of as many as several hundreds core components, including fuel assemblies, blanket assemblies, neutronic shield assemblies, and so on, all of which are submerged in a liquid coolant environment. The subassemblies have the hexagon section and they are very closely spaced each other. The gaps between the subassemblies should be designed to permit removal and insertion of ducts under reactor shutdown conditions, while limiting the free deflection of ducts during normal operation. During a seismic event, these core subassemblies vibrate like cantilevers with load pad impacts under fluid-structure interaction. In this situation, the fluid in the gaps has an important effect on the resulting core seismic responses due to the inertial and viscous coupling of the fluid (IAEA, 1996 ; Koo and Lee, 2001). Recently, the seismic isolation technology (Koo et al., 1999) was introduced to the reactor design to reduce seismic responses. This makes the natural frequency of the reactor pull down to very lower regions. In this situation, the fluid added mass may severely affect the seismic responses.

For simple application of fluid added mass effect, the calculation formulas for various structural sections submerged in inviscid fluids are provided analytically (Fritz, 1972). However, the situation is quite different for the case of viscous fluids, where the fluid field is more complex due to phase change introduced by viscosity. Many researchers have studied the effects of fluid viscosity on vibrating structures with the analytical approach in case of simple sectional shapes (Chen et al., 1976 ; Su, 1983 ; Mulcahy, 1980). In general, the sectional shape of LMFBR core

* Corresponding Author,
E-mail : ghkoo@kaeri.re.kr
TEL : +82-42-868-2950; **FAX** : +82-42-868-8363
Korea Atomic Energy Research Institute, P.O. Box 105, Yusong, Taejon 305-600, Korea. (Manuscript **Received** October 9, 2002; **Revised** December 26, 2002)

subassemblies is a hexagon and the array of these subassemblies is very complicate. To determine the fluid added mass and damping for this actual LMFBR core system, it is not possible deriving the theoretical closed form solution. The numerical approach using the finite element method for circular cylinders has been studied by Newton but this study has dealt with inviscid fluid (Newton et al., 1974). Yang and his colleague have included the fluid viscosity effect in finite element approach using triangular quadratic element type and calculated the fluid added mass and damping coefficients for immersed hexagon cylinders (Yang and Moran, 1980),

In this paper, the numerical finite element formulations were derived for two-dimensional incompressible and homogeneous viscous fluid field and the FAMD (Fluid Added Mass and Damping) code was developed to obtain the fluid added mass and damping for the problems with arbitrary geometric sectional structures submerged in a viscous fluid. In this code, the fluid domain is discretized with C^0-type quadratic quadrilateral elements containing eight nodes; four nodal points at the vertices and four nodal points at the midpoints of the edges. The mixed interpolation method (Zienkiewicz and Taylor, 1991) is introduced in the FAMD code, i.e., the interpolation function for the velocity variable is approximated by a quadratic function based on all eight nodal points and the interpolation function for the pressure variable is approximated by a linear function based on the four nodal points at vertices. As the FAMD pre-processor to generate the analysis input data such as nodal coordinates, element connectives, fluid boundary conditions, and so on, the commercial FEM code, ANSYS was used.

The developed code is very usefully applicable to any arbitrary sections of the immersed structures in fields of reactor core vibration, ship and ocean structure vibration, earthquake engineering, nuclear reactor components design, and so on.

2. Finite Element Formulation of the Governing Equations

To make an approximate approach for the Navier-Stokes' equations in fluid mechanics, the basic assumptions are introduced that 1) fluid is incompressible and homogeneous with density ρ and dynamic viscosity μ, 2) the vibrating motions of the fluid and boundary interfacing with structure are simple harmonic with frequency ω and small amplitude, and 3) all fluid motion is planar. With these assumptions, the Navier-Stokes' equation and continuity equation can be linearized as follows;

$$\rho \frac{\partial v_i}{\partial t}=\rho f_i+\frac{\partial Z_{ij}}{\partial x_j} \tag{1}$$

where

$$\tau_{ij}=-p\delta_{ij}+\mu\left(\frac{\partial v_i}{\partial x_j}+\frac{\partial v_j}{\partial x_i}\right) \tag{2}$$

and

$$\frac{\partial v_i}{\partial x_i}=0 \tag{3}$$

in a fluid domain V.

In Eqs. (1)~(3), v_i represents the velocity components in the x_i direction, where the subscript i has 1 and 2, f_i the body force vector, P the pressure, τ_{ij} the stress tensor, and δ_{ij} the Kronecker delta.

Let v_i^* be the weighting function whose value is zero on the boundary on which the velocity is prescribed and arbitrary elsewhere. The inner product of Eq. (1) and v_i^*, and integral over the fluid domain V becomes

$$\int_V \rho v_i^* \frac{\partial v_i}{\partial t} dV=\int_V \rho v_i^* f_i dV+\int_A \tau_{ij} v_i^* n_j dA - \int_V \tau_{ij} \frac{\partial v_i^*}{\partial x_j} dV,\ i=1, 2 \tag{4}$$

where A appeared in Eq. (4) is the boundary of the fluid domain interfacing with the structure and n_j indicates unit vector in x_i direction.

Weight Eq. (3) with a weighting function p^* whose value is arbitrary on A is

$$\int_V p^* \frac{\partial v_i}{\partial x_i} dV=0 \tag{5}$$

Substitution of Eq. (2) into Eq. (4) gives

$$\int_V \rho v_i^* \frac{\partial v_i}{\partial t} dV - \int_V p \frac{\partial v_i^*}{\partial x_j} \delta_{ij} dV + \int_V \mu \frac{\partial v_i^*}{\partial x_j} \left(\frac{\partial v_i}{\partial x_j} + \frac{\partial v_j}{\partial x_i} \right) dV = \int_V \rho v_i^* f_i dV + \int_A \tau_{ij} v_i^* n_j dA \quad (6)$$

To make a finite element approach, let the velocity and pressure have the following solution forms for each element

$$v_i(x, t) = \sum_{n=1}^{N} \phi^n(x) v_i^n e^{i\omega t} \quad (7)$$

and

$$p(x, t) = \sum_{m=1}^{M} \psi^m(x) p^m e^{i\omega t} \quad (8)$$

where ϕ and ψ are the interpolation function for the velocity and pressure respectively, and the superscripts m and n indicate the local nodal values at nodal number m and n, respectively. N and M indicate the total number of interpolation functions for ϕ and ψ, respectively.

As same manner, the weighting functions v_i^* and p_i^* can be expressed as

$$v_i^*(x, t) = \sum_{n=1}^{N} \phi^n(x) v_i^{*n} e^{i\omega t} \quad (9)$$

and

$$p^*(x, t) = \sum_{m=1}^{M} \psi^m(x) p^{*m} e^{i\omega t} \quad (8)$$

Substitution of Eqs. (7) ~ (10) into Eqs. (5) and (6) gives

$$\int_V p^* \psi \frac{\partial \phi^T}{\partial x_i} v_i dV = 0 \quad (11)$$

and

$$\int_V \rho(i\omega) v_i^* \phi \phi^T v_j dV - \int_V v_i^{*T} \frac{\partial \phi}{\partial x_i} \psi^T p dV + \int_V \mu \left(v_i^{*T} \frac{\partial \phi}{\partial x_j} \frac{\partial \phi^T}{\partial x_j} v_i + v_i^* \frac{\partial \phi}{\partial x_j} \frac{\partial \phi^T}{\partial x_i} v_j \right) dV = \int_V \rho v_i^{*T} \phi f_i dV + \int_A v_i^* \phi \tau_{ij} n_j dA \quad (12)$$

where the superscript T in Eq. (11) and Eq. (12) represents matrix transpose.

For arbitrary weighting function v_i^* and p_i^*, Eq. (12) and Eq. (11) can be rewritten to the following forms:

$$\left[\int_V \rho(i\omega) \phi \phi^T dV \right] v_i - \left[\int_V \frac{\partial \phi}{\partial x_i} \psi^T dV \right] p + \left[\int_V \mu \frac{\partial \phi}{\partial x_j} \frac{\partial \phi^T}{\partial x_j} dV \right] v_i + \left[\int_V \mu \frac{\partial \phi}{\partial x_j} \frac{\partial \phi^T}{\partial x_i} dV \right] v_j = \left[\int_V \rho \phi f_i dV \right] + \left[\int_A \phi \tau_{ij} n_j dA \right] \quad (13)$$

and

$$\left[\int_V \psi \frac{\partial \phi^T}{\partial x_i} dV \right] v_i = 0 \quad (14)$$

Eq. (13) is the expression of the discretized approximation of the linearized Navier-Stokes' equation and Eq. (14) represents the incompressibility condition of fluid. These equations can be simply expressed in the matrix form as

$$\begin{bmatrix} 2A_{11}+A_{22}+i\omega G & A_{21} & -C_1 \\ A_{12} & A_{11}+2A_{22}+i\omega G & -C_2 \\ -C_1^T & -C_2^T & 0 \end{bmatrix} \begin{Bmatrix} v_1 \\ v_2 \\ p \end{Bmatrix} = \begin{Bmatrix} F_1 \\ F_2 \\ 0 \end{Bmatrix} \quad (15)$$

where

$$A_{11} = \left[\int_V \mu \frac{\partial \phi}{\partial x_1} \frac{\partial \phi^T}{\partial x_1} dV \right]_{N \times N}$$

$$A_{22} = \left[\int_V \mu \frac{\partial \phi}{\partial x_2} \frac{\partial \phi^T}{\partial x_2} dV \right]_{N \times N}$$

$$A_{21} = A_{12}^T = \left[\int_V \mu \frac{\partial \phi}{\partial x_2} \frac{\partial \phi^T}{\partial x_1} dV \right]_{N \times N}$$

$$G = \left[\int_V \rho \phi \phi^T dV \right]_{N \times N}$$

$$C_1 = \left[\int_V \frac{\partial \phi}{\partial x_1} \psi^T dV \right]_{N \times M}$$

$$C_2 = \left[\int_V \frac{\partial \phi}{\partial x_2} \psi^T dV \right]_{N \times M}$$

$$F_1 = \left[\int_V \rho \phi f_1 dV + \int_A \phi (\tau_{11} n_1 + \tau_{12} n_2) dA \right]_N$$

$$F_2 = \left[\int_V \rho \phi f_2 dV + \int_A \phi (\tau_{21} n_1 + \tau_{22} n_2) dA \right]_N$$

The stiffness matrix derived in Eq. (15) is square, banded, symmetric, complex, and indefinite. In this paper, the fluid domain is discretized with C^0-type quadratic quadrilateral elements, which is enough to satisfy the convergence and compatibility requirements. Such an element has four nodal points at the vertices and four nodal points at the midpoints of the edges. As expressed in above equations of motion, the degree of derivative of velocity variable is one degree higher than that of the pressure variable. In this situation, if we use the same order of interpolation functions for both velocity and

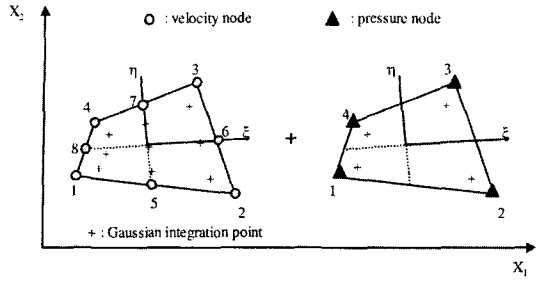

Fig. 1 Used C^0 8-nodes quadratic quadrilateral element for mixed interpolation method

pressure variables, the numerical oscillation can be occurred in solving Eq. (15). To avoid this phenomenon, the mixed interpolation method (Zienkiewicz and Taylor, 1991) is used in this paper. The interpolation function for the velocity variable is approximated by a quadratic function based on all eight nodal points and the interpolation function for the pressure variable is approximated by a linear function based on the four nodal points at vertices as shown in Fig. 1. The complete set of shape functions $[\phi]$ for the velocity variable can be written with isoparametric coordinates ξ and η as

$$\begin{aligned}
\phi_1&=\frac{1}{4}(1-\xi)(1-\eta)-\frac{1}{2}(\phi_8+\phi_5)\\
\phi_2&=\frac{1}{4}(1+\xi)(1-\eta)-\frac{1}{2}(\phi_5+\phi_6)\\
\phi_3&=\frac{1}{4}(1+\xi)(1+\eta)-\frac{1}{2}(\phi_6+\phi_7)\\
\phi_4&=\frac{1}{4}(1-\xi)(1+\eta)-\frac{1}{2}(\phi_7+\phi_8)\\
\phi_5&=\frac{1}{2}(1-\xi^2)(1-\eta),\quad \phi_6=\frac{1}{2}(1+\xi)(1-\eta^2)\\
\phi_2&=\frac{1}{2}(1-\xi^2)(1+\eta),\quad \phi_8=\frac{1}{2}(1-\xi)(1-\eta^2)
\end{aligned} \tag{16}$$

The complete set of shape functions $[\psi]$ for the pressure variable can be written as

$$\begin{aligned}
\psi_1&=\frac{1}{4}(1-\xi)(1-\eta),\quad \psi_2=\frac{1}{4}(1+\xi)(1-\eta)\\
\psi_3&=\frac{1}{4}(1+\xi)(1+\eta),\quad \psi_4=\frac{1}{4}(1-\xi)(1+\eta)
\end{aligned} \tag{17}$$

In terms of interpolation functions, the velocity and pressure variable are approximated by

$$v_i=[\phi]^T\{\mathrm{v}_i\}_e,\ i=1 \text{ and } 2 \tag{18}$$

$$p=[\psi]^T\{\mathrm{p}\}_e \tag{19}$$

where $\{\mathrm{v}_i\}_e^T=\{v_i^1, \cdots, v_i^8\}$ and $\{\mathrm{p}\}_e^T=\{\mathrm{p}^1, \cdots, \mathrm{p}^4\}$ and subscript e means that the vector is base on element.

The used element type has eight nodes with twenty degrees of freedom. Figure 1 shows the definition of degree of freedom in the quadratic quadrilateral element using in this paper. In the integral forms of eq. (15), as no derivatives are present for the pressure component, only the derivatives for the velocity component are to be calculated as follow;

$$\begin{Bmatrix} v_{i,x_1} \\ v_{i,x_2} \end{Bmatrix}=[\mathbf{B}]\{\mathbf{v}_i\}_e \tag{20}$$

where

$$[\mathbf{B}]=\begin{bmatrix} \phi_{1,x_1} & \phi_{2,x_1} & \cdots & \phi_{8,x_1} \\ \phi_{1,x_2} & \phi_{2,x_2} & \cdots & \phi_{8,x_2} \end{bmatrix}$$

In expression of Eq. (20), comma subscribed in variable indicates the partial derivative with respect to following coordinate. The x_1 and x_2 are the orthogonal global coordinate.

The derivatives needed in Eq. (15) are not immediately available because v_i is expressed in terms of ξ and η, not x_1 and x_2. Therefore it is necessary to derive the some relation between the global coordinates and the isoparametric coordinates by sequent operation as follows:

$$\begin{Bmatrix} v_{i,x_1} \\ v_{i,x_2} \end{Bmatrix}=[\Gamma]\begin{Bmatrix} v_{i,\xi} \\ v_{i,\eta} \end{Bmatrix}=[\Gamma][\mathbf{D}]\{\mathbf{v}_i\}_e=[\mathbf{B}]\{\mathbf{v}_i\}_e \tag{21}$$

In above Eq. (21), [D] matrix can be expressed as

$$[\mathbf{D}]=\begin{bmatrix} \phi_{1,\xi} & \phi_{2,\xi} & \cdots & \phi_{8,\xi} \\ \phi_{1,\eta} & \phi_{2,\eta} & \cdots & \phi_{8,\eta} \end{bmatrix} \tag{22}$$

and the $[\Gamma]$ matrix can be obtained by the chain rule,

$$\begin{aligned}
\frac{\partial v_i}{\partial x_1}&=\frac{\partial v_i}{\partial \xi}\frac{\partial \xi}{\partial x_1}+\frac{\partial v_i}{\partial \eta}\frac{\partial \eta}{\partial n_1} \text{ and}\\
\frac{\partial v_i}{\partial x_2}&=\frac{\partial v_i}{\partial \xi}\frac{\partial \xi}{\partial x_2}+\frac{\partial v_i}{\partial \eta}\frac{\partial \eta}{\partial x_2}
\end{aligned} \tag{23}$$

Therefore, $\Gamma_{11}=\xi_{,x}$, $\Gamma_{12}=\eta_{,x}$, $\Gamma_{21}=\xi_{,y}$, $\Gamma_{22}=\eta_{,y}$. In Eq. (23), the partial derivatives of ξ and η with respect to x_1 and x_2 are not directly available. However, the $[\Gamma]$ matrix can be obtained using the expression of Eq. (21) inversely as

$$\frac{\partial v_i}{\partial \xi}=\frac{\partial v_i}{\partial x_1}\frac{\partial x_1}{\partial \xi}+\frac{\partial v_i}{\partial x_2}\frac{\partial x_2}{\partial \xi} \text{ and}$$
$$\frac{\partial v_i}{\partial \eta}=\frac{\partial v_i}{\partial x_1}\frac{\partial x_1}{\partial \eta}+\frac{\partial v_i}{\partial x_2}\frac{\partial x_2}{\partial \eta}$$

or

$$\begin{Bmatrix} v_{i,\xi} \\ v_{i,\eta} \end{Bmatrix}=[\mathbf{J}]\begin{Bmatrix} v_{i,x_1} \\ v_{i,x_2} \end{Bmatrix} \tag{24}$$

where [J] is called the Jacobian matrix :

$$[\mathbf{J}]=\begin{bmatrix} x_{1,\xi} & x_{2,\xi} \\ x_{1,\eta} & x_{2,\eta} \end{bmatrix}=\begin{bmatrix} \sum_{n=1}^{N}(v_i)^n_{,\xi}x_1^n & \sum_{n=1}^{N}(v_i)^n_{,\xi}x_2^n \\ \sum_{n=1}^{N}(v_i)^n_{,\eta}x_1^n & \sum_{n=1}^{N}(v_i)^n_{,\eta}x_2^n \end{bmatrix}$$
$$=[\mathbf{D}]\begin{bmatrix} x_1^1 & x_2^1 \\ x_1^2 & x_2^2 \\ \vdots & \vdots \\ x_1^8 & x_2^8 \end{bmatrix} \tag{25}$$

Therefore, matrix $[\Gamma]$ can be obtained by the inverse of [J],

$$[\Gamma]=[\mathbf{J}]^{-1}=\frac{1}{J}\begin{bmatrix} J_{22} & -J_{12} \\ -J_{21} & J_{11} \end{bmatrix} \tag{26}$$

where J is the determinant of the Jacobian matrix.

With Eqs. (16) ~ (26) and by use of Gauss quadrature formulas over the nine integral points with order 3, each term in Eq. (15) can be integrated exactly. Thus, the element stiffness matrix of Eq. (15) can be obtained and assembled with standard finite element techniques.

3. Determination of Fluid Added Mass and Damping

The fluid added mass and damping of solid bodies submerged in fluid shown in Fig. 2 can be determined for the unit amplitude oscillation of one body in each of two orthogonal directions and no oscillations of the remaining fluid boundaries contacting with other bodies. Each body has hydrodynamic reactions caused by oscillation of itself, other bodies, and the outer container. Therefore, the results of the calculated fluid added mass and damping of solid bodies produce the consistent matrix with complex coupling terms.

In the unit amplitude oscillation of body, the body force is neglected and the shear stress is

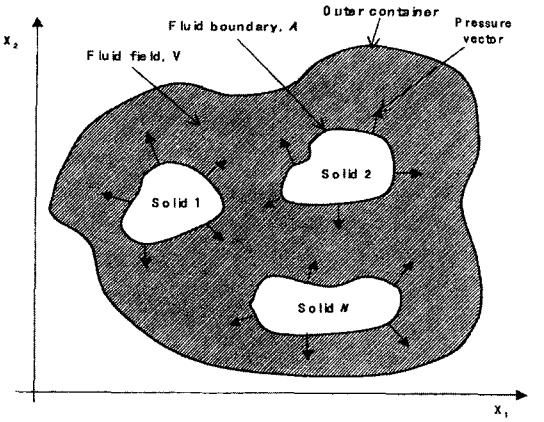

Fig. 2 Two-dimensional fluie field with cross sections of immersed N solid bodies

nowhere prescribed along the fluid boundaries, therefore, F_1 and F_2 in Eq. (15) are zero. To obtain the fluid added mass and damping of solid bodies, the velocity of the fluid boundary oscillating by solid must be prescribed with unit amplitude. In this case, the boundary conditions become

$v_i=U_ie^{i\omega t}$ on fluid boundary at moving body

and

$v_i=0$ on all remaining fluid boundaries (27)

To solve the unknown velocity and pressure vectors in system matrix having prescribed velocity boundary conditions, the system matrix can be partitioned known and unknown vectors as

$$\left[\begin{array}{c|c} \mathbf{K}_{11} & \mathbf{K}_{12} \\ \hline \mathbf{K}_{21} & \mathbf{K}_{22} \end{array}\right]\begin{Bmatrix} \mathbf{w}_1 \\ \mathbf{w}_2 \end{Bmatrix}=\begin{Bmatrix} 0 \\ 0 \end{Bmatrix} \tag{28}$$

where w_1 is a set of prescribed velocity vectors and w_2 is a set of unknown velocity and pressure vectors.

Finally, the unknown vectors can be obtained by solving the following reduced system equation,

$$[\mathbf{K}_{22}]\{\mathbf{w}_2\}=-[\mathbf{K}_{21}]\{\mathbf{w}_1\}=\{C\} \tag{29}$$

The hydrodynamic reaction force acting on the fluid boundaries is calculated using Eq. (2) as follow ;

$$R_i=\int_A \tau_{ij}n_j dA$$
$$=\int_A\{-p\delta_{ij}+\mu(\partial v_i/\partial x_j+\partial v_j/\partial x_i)\}\,n_j dA \tag{30}$$

where the integration carried out over the fluid boundary at each body.

The hydrodynamic reaction force is a complex value and can be expressed in the following form,

$$R_i = Q_i \cos \omega t + iP_i \sin \omega t \qquad (31)$$

In Eq. (31), $P_i \sin \omega t$ component is in phase with the acceleration and $Q_i \cos \omega t$ component is in phase with the velocity. From these components, the fluid added mass, M_f and damping, C_f can be determined as

$$M_f = \frac{P}{\omega U}, \quad C_f = \frac{Q}{U} \qquad (32), (33)$$

For a system with N solid bodies submerged in confined fluid, $2(N+1)$ solutions of Eq. (29) will be carried out and $4(N+1)^2$ integrals of Eq. (30) are required to obtain the consistent fluid added mass and damping matrix for all solid bodies and outer container.

For the dimensionless investigation of the fluid effects, the fluid added mass coefficient, C_m and the fluid damping coefficient, C_v are defined as

$$C_m = \frac{P}{\rho A \omega U}, \quad C_v = \frac{Q}{\rho A \omega U} \qquad (34), (35)$$

4. Examples of Application

4.1 Concentric cylindrical shell

As an example of application, the evaluation of the fluid added mass and damping for the concentric cylindrical shell was carried out. The used fluid properties of the fluid dynamic viscosity and fluid density are $\mu = 9.54 \times 10^{-4}$ N·s/m^2 and $\rho = 1000$ kg/m^3 respectively. The diameter of the inner cylinder is d=15 cm and the diameter ratio of the inner cylinder and outer cylinder is $D/d = 3/\sqrt{3}$.

Figure 3 shows the two-dimensional finite element model of the fluid field for the concentric cylindrical shell. To generate the nodal coordinates, element connectivity, fluid boundary conditions, and so on, the commercial finite element code, ANSYS 5.6 was used.

Figure 4 presents the calculated fluid added mass and damping of the inner cylinder with respect to the Reynolds number $\mathrm{Re} = \rho(\omega d^2/\mu)$.

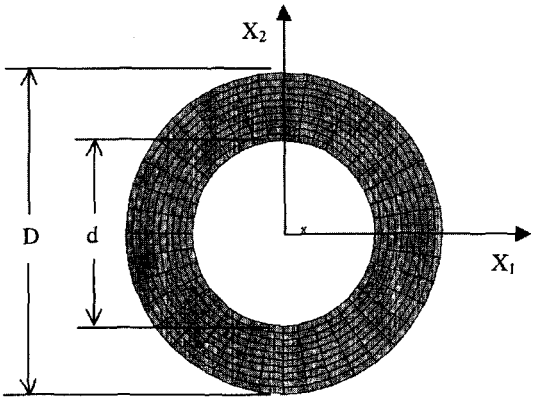

Fig. 3 Finite element model of concentric cylindrical shell

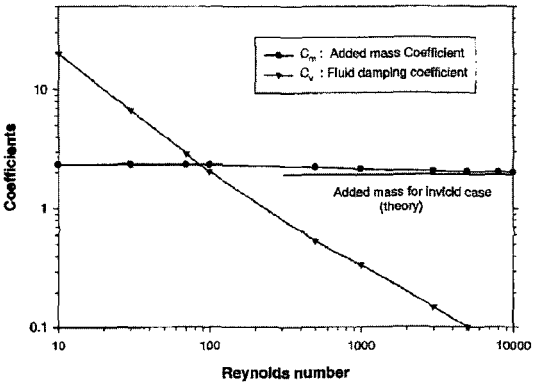

Fig. 4 Calculated fluid added mass and damping for concentric cylindrical shell

As shown in figure, the fluid added mass is larger than the inviscid fluid case due to the fluid viscosity effect. However, as the Reynolds number increases, the fluid added mass coefficient, C_m approaches the value of the inviscid fluid case, which is independent of the excitation frequency, and the fluid damping coefficient, C_v approaches zero.

To verify the FAMD code, the results are compared with those of the theoretical solutions by Fritz for the inviscid fluid case. The fluid added mass matrix for the unit length of concentric cylindrical shell can be obtained using the simple formula as

$$\begin{Bmatrix} F_{x1} \\ F_{x2} \end{Bmatrix} = \begin{bmatrix} \alpha M_1 & -(1+\alpha) M_1 \\ -(1+\alpha) M_1 & (1+\alpha) M_1 + M_2 \end{bmatrix} \begin{Bmatrix} a_{x1} \\ a_{x2} \end{Bmatrix} \qquad (36)$$

Table 1 Fluid added mass matrix of concentric cylindrical shell for inviscid fluid case

		1-X			1-Y			2-X			2-Y		
		100	400	900	100	400	900	100	400	900	100	400	900
1-X	100	34.3						- 51.7					
	400		35.1						−52.7				
	900			35.2 (35.4)						−52.9 (−53.0)			
1-Y	100				34.3						−51.7		
	400					35.1						−52.7	
	900						35.2 (35.4)						−52.9 (−53.0)
2-X	100	−51.7						103.8					
	400		−52.7						105.5				
	900			−52.9 (−53.0)						105.8 (106.0)			
2-Y	100				−51.7						103.8		
	400					−52.7						105.5	
	900						−52.9 (−53.0)						105.8 (106.0)

Note, ( ): Theoretical solutions, 100, 400, 900 ; # of elements, X, Y : global directions

where $\alpha=(R_2^2+R_1^2)/(R_2^2-R_1^2)$, $M_1=\rho\pi R_1^2$, and $M_2=\rho\pi R_2^2$

Table 1 shows the comparison results. The value corresponding to (1-x, 2-x) indicates the fluid force on solid body 1 in the x direction due to the motion of solid body 2 in the x direction. The overall results of the FAMD code are in good agreement with those of theoretical solutions and as the element number increases, the numerical values exactly approach the theoretical solutions.

4.2 Hexagon core of liquid metal reactor

The core of the liquid metal reactor consists of several hundreds hexagon cylinders very closely spaced each other. In this paper, the numerical approach by FAMD code was carried out to investigate characteristics of the fluid added mass and damping for couples of array cases.

4.2.1 Single hexagon system

Figure 5 shows the finite element model of the fluid field for the single-hexagon with outer circular container. The flat to flat diameter of the hexagon is d=15 cm and the diameter ratio of the hexagon and outer container is $D/d=3/\sqrt{3}$ as same as that of previous example for the concentric cylinder.

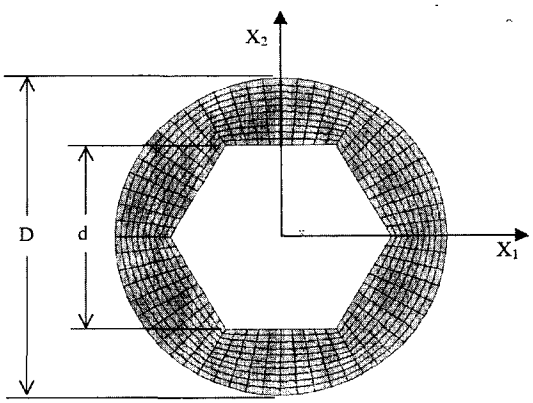

Fig. 5 Finite element model of single hexagon system

Figure 6 gives the calculated results of the fluid added mass and damping coefficients with respect to the Reynolds number. The overall characteristics are same as those of the concentric cylinder but the coefficients are larger. This fact means

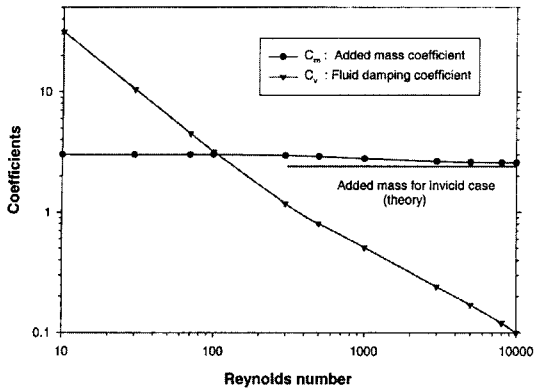

Fig. 6 Calculated fluid added mass and damping for single hexagon system

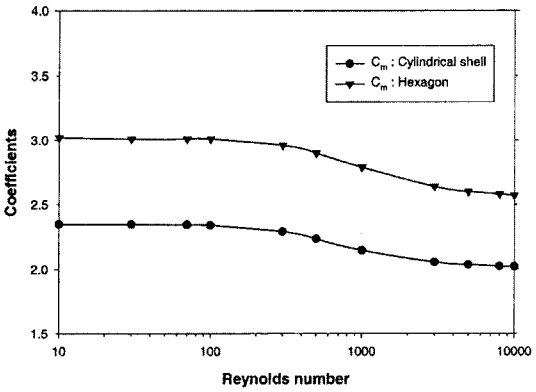

Fig. 7 Comparison of fluid added mass between concentric cylindrical shell and hexagon

that the hexagon section carries the fluid resistance more severely than the circular section. The fluid mass coefficient is larger about 22% as shown in Fig. 7.

4.2.2 Seven-hexagon system

Figure 8 depicts the finite element model of the fluid field for the seven-hexagon system arrayed within an 18-sided regular polygonal boundary and outer circular container. Table 2 and Table 3 reveal the calculated results of the fluid added mass coefficients C_m and the fluid damping coefficient C_v respectively in direction of x_1 for the case of the fluid gap ratio, g/r(=d/2) = 0.06 and the Reynolds number, Re=500. In this result, the center hexagon has the maximum values due to the surrounding thin fluid gap. Figure 9 shows the relationship between the fluid added mass

Table 2 Fluid added mass coefficient, C_m of 7-hexagon for viscous Fluid Case

	1-X	2-X	3-X	4-X	5-X	6-X	7-X
1-X	14.6						
2-X	−3.6	8.6					
3-X	3.1	−1.6	5.7				
4-X	−3.6	−2.0	−1.6	8.6			
5-X	−3.6	−0.8	0.3	3.6	8.6		
6-X	3.1	0.2	0.8	0.2	−1.6	5.7	
7-X	−3.6	3.6	0.3	−0.8	−2.0	−0.5	8.6

Table 2 Fluid damping coefficient, C_v of 7-hexagon for viscous fluid case

	1-X	2-X	3-X	4-X	5-X	6-X	7-X
1-X	300.						
2-X	−95.0	151.					
3-X	40.6	−41.4	49.8				
4-X	−95.0	−44.7	−38.9	151.			
5-X	−95.0	−23.1	−5.7	59.1	151.		
6-X	40.6	−5.9	2.1	−5.9	−41.4	49.8	
7-X	−95.0	59.1	−5.7	−23.1	−44.7	−38.9	151.

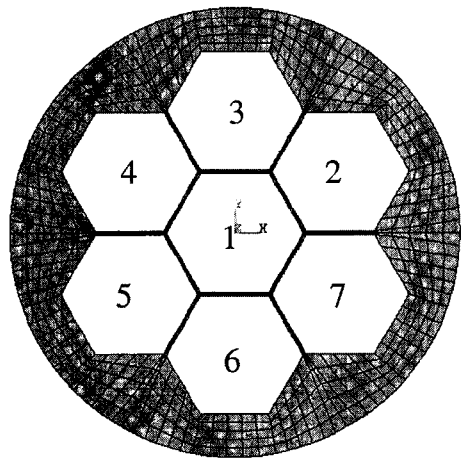

Fig. 8 Finite element model of 7-hexagons system

coefficient, C_m(1-x, 1-x) and the fluid gap for the center hexagon (number 1) in case of Re=500. As shown in figure, the viscous solution gives larger value than those of the potential solution. The discrepancy increases as the fluid gap decreases. This means that the fluid viscosity effect on the fluid added mass becomes to be significant

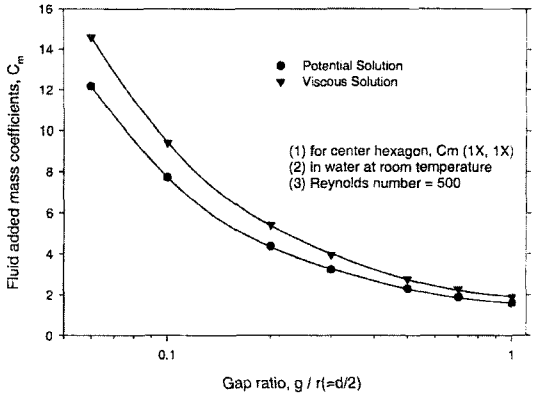

Fig. 9 Fluid added mass coefficient vs. fluid gap ratio for 7-hexagon system

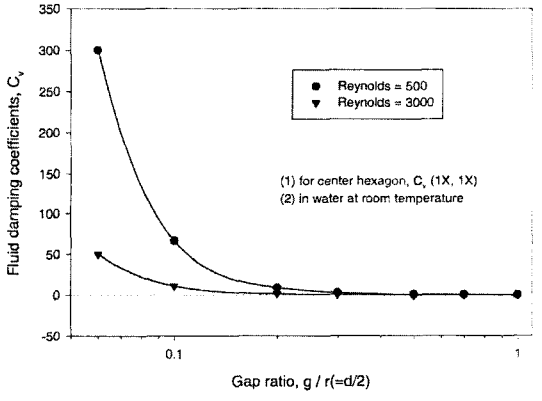

Fig. 10 Fluid damping coefficients vs. fluid gap ratio for 7-hexagon system

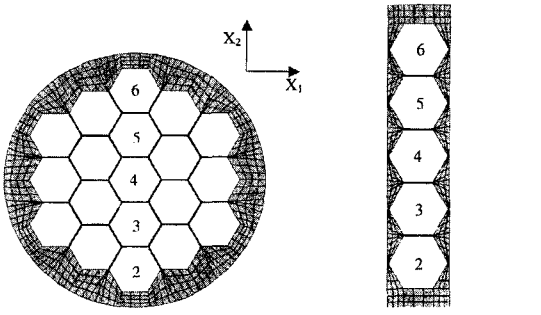

(a) Group 19-hexagons model (b) Single row 5-hexagons model

Fig. 11 Finite element models used in analyses

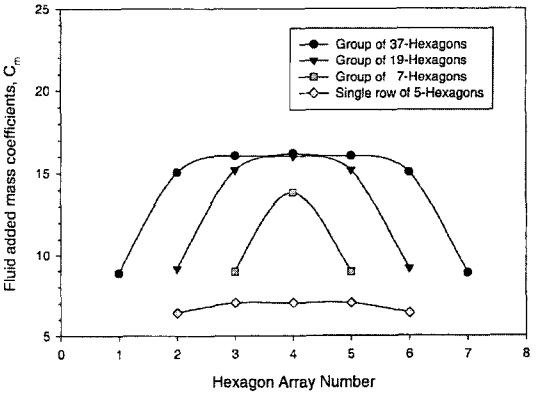

Fig. 12 Comparison of fluid added mass coefficients of central hexagons for various models in direction of x_2

when the fluid gap is small. When the fluid gap decreases, C_m increases exponentially and as the fluid gap increases, C_m approaches constant value having no fluid gap effect. Figure 10 shows the relationship between the fluid damping coefficients and the fluid gap for the center hexagon in two cases of Re=500 and Re=3000. As the fluid gap ratio, g/r increases, C_v approaches zero. At small gap regions, we can see that the effect of the Reynolds number becomes very sensitive on the fluid damping coefficient.

4.2.3 Muti-hexagon and single row hexagon system

Actually, it is very difficult to obtain the whole matrix of the fluid added mass and damping for several hundreds duct assemblies due to the finite element modeling size and computing time. In this paper, the effects of the number of hexagons are investigated for the inviscid case.

Figure 11 depicts the finite element models for group of 19-hexagon system and simple single row hexagon system for a central array. Figure 12 shows the calculated results of the fluid added mass coefficient for the single row hexagon array as shown in Fig. 11. From the results, it is known that the fluid added mass of a single row model is much smaller than those of the group models. Therefore, it should be careful in seismic tests with the conventional single row model, which may result in significant discrepancy compared with full core system. With increase the number of hexagons over 19, outermost hexagons do not affect the fluid added mass of the inner hexagons and the fluid added mass coefficient converged to

constant value at most inside hexagons. This fact indicates that the fluid added mass of the LMR core should be estimated using the group of 37-hexagon system at least.

5. Conclusions

In this paper, the finite element formulations for calculating the fluid added mass and damping for arbitrary sectional structure submerged in a viscous fluid are derived and the computer program FAMD code is developed for the practical applications. From the results of concentric cylindrical shell, it is verified that the FAMD code gives good agreements compared with those of theoretical solutions. The results for actual system of the liquid metal reactor core indicate that viscous effects become to be significant and the fluid damping is very sensitive to the Reynolds number for small fluid gap conditions. From the comparison results between the group hexagon model and the single row model of the reactor core, the group model gives much larger fluid added mass than the single row model.

Acknowledgment

This work has been carried out under the Nuclear R&D Program by MOST in Korea.

References

ANSYS User's Manual for Revision 5.6, Volume I, II, III.

Chen, S. S. Wambsganss, M. W. and Jendrzejczyk, J. A., 1976, "Added Mass and Damping of a Vibrating Rod in Confined Viscous Fluid," *Journal of Applied Mechanics*, Vol. 98, pp. 325~329.

Fritz, R. J., 1972, "The Effect of Liquids on the Dynamic Motions of Immersed Solids," *Journal of Engineering for Industry, Transactions of the ASME*, pp. 167-173.

Intercomparison of Liquid metal Fast Reactor Seismic Analysis Codes, Volume 3 : Comparison of Observed Effects with Computer Simulated Effects on Reactor Cores from Seismic Disturbances, *IAEA-TECDOC-882*, IAEA, 1996.

Koo, G. H. Lee, J. H. Lee, H. Y. and Yoo, B., 1999, "Stability of Laminated Rubber Bearing and its Application to Seismic Isolation," *KSME International Journal*, Vol. 13, No. 8, pp. 595~604.

Koo, G. H. and Lee, J. H., 2001, "Effect of Fluid Added Mass on Vibration Characteristics and Seismic Responses of Immersed Concentric Cylinders," *Journal of the Earthquake Engineering Society of Korea*, Vol. 5, No. 5, pp. 25~33.

Mulcahy, T. M., 1980, "Fluid Forces on Rods Vibrating in Finite Length Annular Regions," *Journal of Applied Mechanics*, Vol. 47, pp. 234~240.

Newton, R. E., Chenault, D. W. and Smith, D. A., 1974, "Finite Element Solution for Added Mass and Damping," *Proceedings of the Int. Sym. on Finite Element Methods in Flow Problems*, Swansea.

Su, T. C., 1983, "The Effect of Viscosity on the Forced Vibrations of Fluid-Filled Elastic Shell," *Journal of Applied Mechanics*, Vol. 50, pp. 517~524.

Yang, C. I., and Moran, T. J., 1980, "Calculations of Added Mass and Damping Coefficients for Hexagonal Cylinders in a Confined Viscous Fluid," *Journal of Pressure Vessel Technology*, Vol. 102, pp. 152~157.

Zienkiewicz and Taylor, 1991, *The Finite Element Method*, Fourth Edition, Volume 2, Solid and Fluid Mechanics, Dynamics and Non-linearity, *McGRAW-HILL*.